Published for SISSA by Springer

Received: November 26, 2022
Revised: March 5, 2023
Accepted: March 8, 2023
Published: March 22, 2023

Constraints on the doublet left-right symmetric model from Higgs data

Siddhartha Karmakar,[a,b] **Jai More,**[a] **Akhila Kumar Pradhan**[a] **and S. Uma Sankar**[a]

[a] *Department of Physics, Indian Institute of Technology Bombay, Powai, Mumbai-400076, India*

[b] *Department of Theoretical Physics, Tata Institute of Fundamental Research, Colaba, Mumbai-400005, India*

E-mail: siddhartha.karmakar_315@tifr.res.in, more.physics@gmail.com, akhilpradhan@iitb.ac.in, uma@phy.iitb.ac.in

Abstract: We study the constraints on the doublet left-right symmetric model (DLRSM) arising due to the Higgs data. The $SU(2)_L$ symmetry of this model is broken by three vacuum expectation values, κ_1, κ_2 and v_L. Most studies of this model assume that the ratios $r = \kappa_2/\kappa_1$ and $w = v_L/\kappa_1$ are very small. In this work, we study the constraints imposed on r and w by the Higgs data from LHC. We consider the most general scalar potential and calculate the masses of the CP-even scalars and the couplings of the lightest of these scalars to itself, to W and Z gauge bosons and to the third generation quarks. We find that there is no lower bound on either r or w. Equating the mass of the lightest CP-even scalar to 125 GeV leads to an upper limit $w < 6.7$. The requirement that the Yukawa coupling of the quarks to the Higgs bidoublet of the model should be perturbative yields the upper bounds $r < 0.8$ and $w < 3.5$. The Yukawa coupling of the bottom quark to the lightest CP-even scalar strongly disfavours value of $r, w < 0.1$ and shows a marked preference for values of $w \sim \mathcal{O}(1)$.

Keywords: Higgs Properties, Left-Right Models

ArXiv ePrint: 2211.08445

https://doi.org/10.1007/JHEP03(2023)168

JHEP03(2023)168

Contents

JHEP03(2023)168

1 Introduction

Left-right symmetric models, based on the symmetry group $\mathrm{SU}(2)_L \times \mathrm{SU}(2)_R \times \mathrm{U}(1)_{\mathrm{B-L}}$, have been attractive candidates for physics beyond the standard model (SM) [1–5]. In these models, the left-chiral fermions are doublets under $\mathrm{SU}(2)_L$ and singlets under $\mathrm{SU}(2)_R$. The situation is reversed for the right-chiral fermions. The $\mathrm{U}(1)_{\mathrm{B-L}}$ hyper-charges of the fermions are fixed by the modified Gell-Mann-Nishijima formula connecting them to their respective electric charges. These models have been deployed to address numerous open problems of particle physics, such as neutrino mass generation, dark matter, unification of forces, etc.

The scalar sector of this model requires a minimum of three different Higgs multiplets. Fermion mass generation requires a scalar bidoublet Φ, which transforms as a doublet

under both $SU(2)_L$ and $SU(2)_R$. In addition, we need two more scalar multiplets to break the gauge symmetry of the model to $U(1)_{em}$ and to maintain the left-right symmetry of the Lagrangian. These additional scalars can be either SU(2) doublets or triplets. In doublet left-right symmetric models (DLRSM), they are denoted as χ_L (χ_R) which is a doublet (singlet) under $SU(2)_L$ and a singlet (doublet) under $SU(2)_R$. When the neutral component of χ_R acquires the vacuum expectation value (*vev*) v_R, the symmetry of the model is broken to that of the SM. When the neutral components of χ_L and Φ acquire *vev*s, the symmetry is finally broken to $U(1)_{em}$. Since there is no evidence yet for any right-handed currents in weak interactions, the value of v_R has to be much greater than the *vev*s of χ_L and Φ. If the additional scalars are SU(2) triplets, the model is called triplet left-right symmetric model (TLRSM). In this model, it is possible to generate light Majorana masses for neutrinos, through both type-I and type-II see-saw mechanisms. The constraints on the scalar sector of this model are qualitatively different from those of DLRSM. In this work, we confine our attention to DLRSM.

The minimal form of DLRSM was originally discussed in ref. [5]. Ref. [6] extended this model by adding a singly-charged SU(2) singlet complex scalar so that small neutrino masses can be generated at one-loop level by the Zee mechanism [7]. Such a scalar mixes with the charged scalars in DLRSM. The details of this mixing are constrained from the neutrino oscillation data [8], flavour violating decays of charged leptons [9], and collider searches for RH neutrinos [10].

It is an interesting question to ask what the dominant source of electroweak symmetry breaking (EWSB) in DLRSM is: whether it is the *vev* v_L of the doublet χ_L or the *vev*s κ_1 and κ_2 of the bidoublet Φ. Most models, based on left-right symmetry, assume the latter to be the case. By considering the bounds from perturbative unitarity of scalar and gauge boson scattering and the electroweak precision data, ref. [11] showed that both the above possibilities are allowed. It means there is no hierarchy between v_L and κ_1, κ_2. Most left-right symmetric models also assume $\kappa_2 \ll \kappa_1$. It will be interesting to see what bounds the data imposes on this hierarchy. The purpose of the current study is to analyse the pattern of EWSB in the simplest DLRSM in light of Higgs data and theoretical arguments such as perturbativity, unitarity, and boundedness from below.

In section 2 we introduce our notations and discuss the key features of the different sectors of DLRSM. In section 3 we mention the bounds from perturbativity, unitarity, and boundedness from below. A convenient and minimal basis of quartic parameters have been introduced in section 4. Salient features of the model in light of Higgs data are presented in section 5. This section also discusses the validity of the assumption of hierarchy in the *vev*s $v_L, \kappa_2 \ll \kappa_1$ as a function of the values of the quartic couplings in the model. We make our concluding remarks in section 6.

2 The doublet left-right symmetric model: essentials and notations

DLRSM is based on the gauge symmetry $SU(3)_C \times SU(2)_L \times SU(2)_R \times U(1)_{B-L}$. The fermion content of the model is given below, where the parenthesis contain the quantum

JHEP03(2023)168

numbers of the fermions under each of the sub-groups of the gauge group,

$$Q_L = \begin{pmatrix} u_L \\ d_L \end{pmatrix} \sim (3,2,1,1/3), \qquad Q_R = \begin{pmatrix} u_R \\ d_R \end{pmatrix} \sim (3,1,2,1/3),$$
$$L_L = \begin{pmatrix} \nu_L \\ e_L \end{pmatrix} \sim (1,2,1,-1), \qquad L_R = \begin{pmatrix} \nu_R \\ e_R \end{pmatrix} \sim (1,1,2,-1). \tag{2.1}$$

For any left-right symmetric model, parity is truly manifest as a symmetry, making the Lagrangian symmetric under transformations $Q_L \leftrightarrow Q_R$, $L_L \leftrightarrow L_R$. Note that the model necessarily contains a right-handed neutrino ν_R, which is required to complete the lepton doublet. Both ν_L and ν_R receive Majorana masses if DLRSM is extended with additional scalars [9] or fermions [12]. In our work, we do not include these additional fields.

2.1 The scalar potential

The scalar sector consists of a complex bidoublet and two doublets with the following charges under the aforementioned gauge group

$$\Phi = \begin{pmatrix} \phi_1^0 & \phi_2^+ \\ \phi_1^- & \phi_2^0 \end{pmatrix} \sim (1,2,2,0), \;\; \chi_L = \begin{pmatrix} \chi_L^+ \\ \chi_L^0 \end{pmatrix} \sim (1,2,1,1), \;\; \chi_R = \begin{pmatrix} \chi_R^+ \\ \chi_R^0 \end{pmatrix} \sim (1,1,2,1)\,,$$

with the *vev* structure

$$\langle \Phi \rangle = \frac{1}{\sqrt{2}} \begin{pmatrix} \kappa_1 & 0 \\ 0 & \kappa_2 \end{pmatrix}, \qquad \langle \chi_L \rangle = \frac{1}{\sqrt{2}} \begin{pmatrix} 0 \\ v_L \end{pmatrix}, \qquad \langle \chi_R \rangle = \frac{1}{\sqrt{2}} \begin{pmatrix} 0 \\ v_R \end{pmatrix}. \tag{2.2}$$

The spontaneous breaking of $\mathrm{SU}(2)_R \times \mathrm{U}(1)_{B-L} \to \mathrm{U}(1)_Y$ is driven by the *vev* of the doublet χ_R whereas the EWSB is triggered by the three *vevs* κ_1, κ_2, and v_L. The last three *vevs* are constrained by $\kappa_1^2 + \kappa_2^2 + v_L^2 = v^2$, where $v = 246\,\mathrm{GeV}$. For later use, it is convenient to introduce the ratios $r = \kappa_2/\kappa_1$ and $w = v_L/\kappa_1$. The *vevs* of the scalars must have the hierarchy $v_R \gg v$, which ensures that the gauge bosons of $\mathrm{SU}(2)_R$ are much heavier than the weak gauge bosons. The Yukawa couplings of the bidoublet with fermions lead to fermion masses and mixings. The details of these couplings will be discussed later in section 2.4.

The most general, CP-conserving, renormalizable Higgs potential involving Φ, χ_L and χ_R fields is given by

$$\begin{aligned}
V &= V_2 + V_3 + V_4, \\
V_2 &= -\mu_1^2 \mathrm{Tr}(\Phi^\dagger\Phi) - \mu_2^2 \left[\mathrm{Tr}(\tilde{\Phi}\Phi^\dagger) + \mathrm{Tr}(\tilde{\Phi}^\dagger\Phi)\right] - \mu_3^2 \left[\chi_L^\dagger\chi_L + \chi_R^\dagger\chi_R\right], \\
V_3 &= \mu_4 \left[\chi_L^\dagger\Phi\chi_R + \chi_R^\dagger\Phi^\dagger\chi_L\right] + \mu_5 \left[\chi_L^\dagger\tilde{\Phi}\chi_R + \chi_R^\dagger\tilde{\Phi}^\dagger\chi_L\right], \\
V_4 &= \lambda_1 \mathrm{Tr}(\Phi^\dagger\Phi)^2 + \lambda_2 \left[\mathrm{Tr}(\tilde{\Phi}\Phi^\dagger)^2 + \mathrm{Tr}(\tilde{\Phi}^\dagger\Phi)^2\right] + \lambda_3 \mathrm{Tr}(\tilde{\Phi}\Phi^\dagger)\,\mathrm{Tr}(\tilde{\Phi}^\dagger\Phi) \\
&\quad + \lambda_4 \mathrm{Tr}(\Phi^\dagger\Phi)\left[\mathrm{Tr}(\tilde{\Phi}\Phi^\dagger) + \mathrm{Tr}(\tilde{\Phi}^\dagger\Phi)\right] + \rho_1 \left[(\chi_L^\dagger\chi_L)^2 + (\chi_R^\dagger\chi_R)^2\right] + \rho_2\, \chi_L^\dagger\chi_L\chi_R^\dagger\chi_R \\
&\quad + \alpha_1 \mathrm{Tr}(\Phi^\dagger\Phi)[\chi_L^\dagger\chi_L + \chi_R^\dagger\chi_R] + \left\{\alpha_2 \left[\chi_L^\dagger\chi_L \mathrm{Tr}(\tilde{\Phi}\Phi^\dagger) + \chi_R^\dagger\chi_R \mathrm{Tr}(\tilde{\Phi}^\dagger\Phi)\right] + \mathrm{h.c.}\right\} \\
&\quad + \alpha_3 \left[\chi_L^\dagger\,\Phi\Phi^\dagger\chi_L + \chi_R^\dagger\Phi^\dagger\Phi\chi_R\right] + \alpha_4 \left[\chi_L^\dagger\,\tilde{\Phi}\tilde{\Phi}^\dagger\chi_L + \chi_R^\dagger\tilde{\Phi}^\dagger\tilde{\Phi}\chi_R\right].
\end{aligned} \tag{2.3}$$

Here all the couplings can be made real by appropriate field redefinitions.

JHEP03(2023)168

The following conditions minimize the potential

$$\frac{\partial V}{\partial \kappa_1} = \frac{\partial V}{\partial \kappa_2} = \frac{\partial V}{\partial v_L} = \frac{\partial V}{\partial v_R} = 0\,. \tag{2.4}$$

We utilize these conditions to replace the four mass parameters $\mu_1^2, \mu_2^2, \mu_3^2$ and μ_5 by the *vev*s and quartic couplings,

$$\begin{aligned}
\mu_1^2 &= \frac{1}{2(r^2-1)}\bigg(\kappa_1^2\Big(w^2((r^2-1)\alpha_1 + r^2\alpha_3 - \alpha_4) + 2(r^2-1)((r^2+1)\lambda_1 + 2r\lambda_4)\Big) \\
&\quad + 2\sqrt{2}rv_R w\mu_4 + v_R^2\Big((r^2-1)\alpha_1 + r^2\alpha_3 - \alpha_4 + 2w^2\rho_{12}\Big)\bigg)\,, \\
\mu_2^2 &= \frac{1}{4(r^2-1)}\bigg(\kappa_1^2\Big(w^2(r^2-1)\alpha_2 - w^2 r\alpha_{34} + 2(r^2-1)(2r\lambda_{23} + (r^2+1)\lambda_4)\Big) \\
&\quad - \sqrt{2}(r^2+1)v_R w\mu_4 + v_R^2\Big((r^2-1)\alpha_2 - r\alpha_{34} - 2w^2\rho_{12}\Big)\bigg)\,, \\
\mu_3^2 &= \frac{1}{2}\kappa_1^2((r^2+1)\alpha_1 + 2r\alpha_2 + r^2\alpha_3 + \alpha_4 + 2w^2\rho_1) + v_R^2\rho_1\,, \\
\mu_5 &= -r\mu_4 - \sqrt{2}v_R w\rho_{12}\,.
\end{aligned} \tag{2.5}$$

Here $\rho_{12} = \rho_2/2 - \rho_1$, $\alpha_{34} = \alpha_3 - \alpha_4$, and $\lambda_{23} = 2\lambda_2 + \lambda_3$. From the definition of r and w, we note that $\kappa_1^2(1 + r^2 + w^2) = v^2$. That is, the value of κ_1 is fixed for a given r and w. Thus the parameters of the DLRSM scalar sector are

$$\{\lambda_{1,2,3,4}, \alpha_{1,2,3,4}, \rho_{1,2}, \mu_4, r, w, v_R\}\,. \tag{2.6}$$

Among these, the only dimensionful parameter is μ_4. For most of the following discussions, we will either set it to zero or restrict it to $\mu_4 \lesssim v_R$.

2.2 The gauge sector

The charged gauge boson mass matrix in this model is

$$\mathcal{L}_{\rm mass} \supset \begin{pmatrix} W_L^+ & W_R^+ \end{pmatrix} \begin{pmatrix} \frac{g_L^2}{4}(v_L^2 + \kappa_1^2 + \kappa_2^2) & -\frac{1}{2}g_L g_R \kappa_1\kappa_2 \\ -\frac{1}{2}g_L g_R \kappa_1\kappa_2 & \frac{g_R^2}{4}(v_R^2 + \kappa_1^2 + \kappa_2^2) \end{pmatrix} \begin{pmatrix} W_L^- \\ W_R^- \end{pmatrix}. \tag{2.7}$$

Here $g_{L(R)}$ are the gauge couplings associated with $\mathrm{SU}(2)_{L(R)}$. The physical charged gauge bosons have masses

$$m_{W_{1,2}}^2 = \frac{1}{8}\Big(g_L^2 v^2 + g_R^2 V^2 \mp \sqrt{(g_L^2 v^2 - g_R^2 V^2)^2 + 16 g_L^2 g_R^2 \kappa_1^2 \kappa_2^2}\Big)\,, \tag{2.8}$$

where $W_1^\pm$ is close to the SM $W^\pm$ boson and W_2 has mass of the order of v_R. The mixing between $W_L^\pm$ and $W_R^\pm$ given by

$$\begin{pmatrix} W_L^\pm \\ W_R^\pm \end{pmatrix} = \begin{pmatrix} \cos\xi & -\sin\xi \\ \sin\xi & \cos\xi \end{pmatrix} \begin{pmatrix} W_1^\pm \\ W_2^\pm \end{pmatrix},$$

JHEP03(2023)168

where

$$\tan\xi = \frac{4g_L g_R \kappa_1 \kappa_2}{g_L^2 v^2 - g_R^2 V^2 - \sqrt{(g_L^2 v^2 - g_R^2 V^2)^2 + 16 g_L^2 g_R^2 \kappa_1^2 \kappa_2^2}}\,. \tag{2.9}$$

Here, we adhere to the definitions, $v^2 = \kappa_1^2 + \kappa_2^2 + v_L^2$ and $V^2 = \kappa_1^2 + \kappa_2^2 + v_R^2$. In the limit $\kappa_1, \kappa_2, v_L \ll v_R$ and $g_L = g_R$, the mixing angle becomes $\xi \simeq -2\kappa_1\kappa_2/v_R^2$.

In a similar fashion, the neutral gauge boson mass matrix can be written as

$$\mathcal{L}_{\text{mass}} \supset \frac{1}{8}\begin{pmatrix} W_{L\mu}^3 & W_{R\mu}^3 & B_\mu \end{pmatrix} \begin{pmatrix} g_L^2 v^2 & -g_L g_R \kappa_+^2 & -g_L g_{BL} v_L^2 \\ & g_R^2 V^2 & -g_R g_{BL} v_R^2 \\ & & g_{BL}^2 (v_L^2 + v_R^2) \end{pmatrix} \begin{pmatrix} W_{L\mu}^3 \\ W_{R\mu}^3 \\ B_\mu \end{pmatrix}, \tag{2.10}$$

with the mass eigenvalues

$$\begin{aligned} m_{Z_1,Z_2}^2 = \frac{1}{8}\Big(& g_L^2 v^2 + g_R^2 V^2 + g_{BL}^2 (v_L^2 + v_R^2) \\ & \mp \sqrt{(g_L^2 v^2 + g_R^2 V^2 + g_{BL}^2 (v_L^2 + v_R^2))^2 + 4(g_L^2 g_R^2 + g_L^2 g_{BL}^2 + g_R^2 g_{BL}^2)(\kappa_+^4 - v^2 V^2)}\Big)\,, \end{aligned} \tag{2.11}$$

where $\kappa_+^2 = \kappa_1^2 + \kappa_2^2$ and g_{BL} is the gauge coupling of $\mathrm{U}(1)_{B-L}$. The lighter boson Z_1 is close to the SM Z boson and the heavier boson Z_2 has a mass of order v_R. The exact expressions for the mass eigenstates in terms of the gauge eigenstates are given in appendix A.

In the limit $\kappa_1, \kappa_2, v_L \ll v_R$ and $g_L = g_R = g$ the mixing reduces to [13]

$$\begin{pmatrix} A_\mu \\ Z_{1\mu} \\ Z_{2\mu} \end{pmatrix} = \begin{pmatrix} s_W & c_W s_Y & c_W c_Y \\ -c_W & s_W s_Y & s_W c_Y \\ 0 & c_Y & s_Y \end{pmatrix} \begin{pmatrix} W_{L\mu}^3 \\ W_{R\mu}^3 \\ B_\mu \end{pmatrix}, \tag{2.12}$$

where

$$\begin{aligned} s_W \equiv \sin\theta_W = \frac{g_{BL}}{\sqrt{g^2 + 2g_{BL}^2}}\,, \quad c_W \equiv \cos\theta_W = \sqrt{\frac{g^2 + g_{BL}^2}{g^2 + 2g_{BL}^2}}\,, \\ s_Y \equiv \sin\theta_Y = \frac{g_{BL}}{\sqrt{g^2 + g_{BL}^2}}\,, \qquad c_Y \equiv \cos\theta_Y = \frac{g}{\sqrt{g^2 + g_{BL}^2}}\,. \end{aligned} \tag{2.13}$$

In the remainder of the paper we will assume manifest LR symmetry in the gauge sector leading to $g_L = g_R = g$.

If we retain only v_R^2 terms in eqs. (2.8) and (2.11), we find $m_{W_2} = gv_R/2$ and $m_{Z_2} = m_{W_2}/\cos\theta_Y$. The present experimental lower limits on charged heavy gauge boson is $m_{W'} \geq 6$ TeV [14], obtained under the assumption that fermions couple to W' and to the usual W with the same strength. This assumption is certainly valid for manifest DLRSM. Since $v_R \approx 2m_{W_2}/g$, we must have $v_R \sim 20$ TeV to satisfy the experimental lower bound on m_{W_2}. The experimental lower bound on neutral heavy gauge boson is $m_{Z'} \geq 5.1$ TeV [15, 16], which again is obtained under the assumption that the fermions couple to Z' and to the usual Z with the same strength. Such an assumption is approximately true for

JHEP03(2023)168

manifest DLRSM. Since the predicted value of m_{Z_2} is greater than the predicted value of m_{W_2}, the lower bound on m_{Z_2} is automatically satisfied if the lower bound on m_{W_2} is satisfied. Our numerical calculations give the values $m_{W_2} = 6.5$ TeV and $m_{Z_2} = 7.7$ TeV for $v_R = 20$ TeV. When the SU(2)$_L$ breaking *vevs*, κ_1, κ_2 and v_L are varied subject to the constraint $\kappa_1^2 + \kappa_2^2 + v_L^2 = v^2$, the changes in m_{W_2} and m_{Z_2} are less than 1%.

2.3 CP-even neutral scalars

The experiments at LHC have measured the mass of the Higgs boson and its couplings to gauge bosons and fermions. They have also set lower limits on masses of heavy neutral and charged scalars. The aim of this work is to utilize the Higgs boson measurements to constrain the parameters of DLRSM. So we study the CP-even neutral scalars of DLRSM in detail. For completeness, we have included the masses of CP-odd neutral scalars and charged scalars in appendix A.

The gauge and physical bases for the CP-even neutral scalars are $X = (\phi_{1r}^0, \phi_{2r}^0, \chi_{Lr}^0, \chi_{Rr}^0)$ and $X_{\rm ph} = (h, H_1, H_2, H_3)$ respectively. Here h is the lightest CP-even scalar with mass of the order of v and $H_i\,(i = 1, 2, 3)$ are heavier scalars with masses of the order of v_R. It is expected that the properties of h will be very similar to those of SM Higgs boson.

The mass matrix for scalars in the gauge basis is denoted by M^2. It can be decomposed in powers of v_R which enables the use of perturbation theory due to the hierarchy of scales $\kappa_1, \kappa_2, v_L \ll v_R$,

$$M^2 = \left(M^{2\,(0)} v_R^2 + M^{2\,(1)} v_R + M^{2\,(2)}\right), \tag{2.14}$$

where $M^{2\,(0)}$, $M^{2\,(1)}$ and $M^{2\,(2)}$ are three symmetric matrices. The eigenvalues of this matrix must be positive, because they represent the masses of the scalars. The explicit forms of these symmetric components are

$$\begin{aligned}
(M^{2\,(2)})_{11} &= \frac{1}{2}\kappa_1^2(w^2(\alpha_1+\alpha_4) + 2(3+r^2)\lambda_1 + 4r(r\lambda_{23} + 3\lambda_4))\,,\\
(M^{2\,(2)})_{12} &= \frac{1}{2}\kappa_1^2(w^2\alpha_2 + 4r(\lambda_1 + 2\lambda_{23}) + 6(r^2+1)\lambda_4)\,,\\
(M^{2\,(2)})_{13} &= w\kappa_1^2(\alpha_1 + r\alpha_2 + \alpha_4)\,, \quad (M^{2\,(0)})_{14} = -\frac{rw\kappa_1\mu_4}{\sqrt{2}}\,,\\
(M^{2\,(2)})_{22} &= \frac{1}{2}\kappa_1^2(w^2(\alpha_1+\alpha_3) + 2(3r^2+1)\lambda_1 + 4(\lambda_{23} + 3r\lambda_4))\,,\\
(M^{2\,(2)})_{23} &= w\kappa_1^2(\alpha_2 + r(\alpha_1+\alpha_3))\,,\ (M^{2\,(0)})_{24} = \frac{w\kappa_1\mu_4}{\sqrt{2}}\,,\\
(M^{2\,(2)})_{33} &= \frac{1}{2}\kappa_1^2((r^2+1)\alpha_1 + 2r\alpha_2 + r^2\alpha_3 + \alpha_4 + 6w^2\rho_1)\,, \quad (M^{2\,(2)})_{34} = 0\,,\\
(M^{2\,(2)})_{44} &= \frac{1}{2}\kappa_1^2((r^2+1)\alpha_1 + 2r\alpha_2 + r^2\alpha_3 + \alpha_4 + w^2\rho_2)\,,
\end{aligned} \tag{2.15}$$

$$M^{2\,(1)} = \begin{pmatrix}
\frac{\sqrt{2}rw\mu_4}{1-r^2} & -\frac{(r^2+1)w\mu_4}{\sqrt{2}(1-r^2)} & -\frac{r\mu_4}{\sqrt{2}} & \kappa_1((\alpha_1 + r\alpha_2 + \alpha_4) - w^2\rho_{12}) \\
 & \frac{\sqrt{2}rw\mu_4}{1-r^2} & \frac{\mu_4}{\sqrt{2}} & \kappa_1(\alpha_2 + r(\alpha_1+\alpha_3)) \\
 & & 0 & w\kappa_1(\rho_1 + \rho_2/2) \\
 & & & 0
\end{pmatrix}, \tag{2.16}$$

JHEP03(2023)168

$$M^{2\,(0)} = \begin{pmatrix} \frac{r^2\alpha_{34}+2w^2\rho_{12}}{2(1-r^2)} & \frac{r(\alpha_{34}+2w^2\rho_{12})}{2(1-r^2)} & -w\rho_{12} & 0 \\ & \frac{\alpha_{34}+2w^2\rho_{12}}{2(1-r^2)} & 0 & 0 \\ & & \rho_{12} & 0 \\ & & & 2\rho_1 \end{pmatrix}, \tag{2.17}$$

where, for convenience, only the upper halves of the matrices $M^{2\,(1)}$ and $M^{2\,(0)}$ are displayed in eqs. (2.16) and (2.17) respectively.

Since the smallest eigenvalue of M^2 must be of order v^2, its expression must not contain any positive powers of v_R. Hence both $M^{2\,(0)}$ and $M^{2\,(1)}$ must have zero as their smallest eigenvalues. The other three eigenvalues of M^2 correspond to (mass)^2 of heavy CP-even scalars. This requires the non-zero eigenvalues of $M^{2\,(0)}$ to be positive.

We aim to calculate the smallest eigenvalue of M^2 using perturbation theory. First we apply a similarity transformation on M^2, using the orthogonal matrix [8] which diagonalizes $M^{2\,(0)}$,

$$O_I = \begin{pmatrix} \frac{1}{k} & \frac{r}{k} & \frac{w}{k} & 0 \\ -\frac{r}{\sqrt{1+r^2}} & -\frac{1}{\sqrt{1+r^2}} & 0 & 0 \\ -\frac{w}{k\sqrt{1+r^2}} & -\frac{rw}{k\sqrt{1+r^2}} & -\frac{\sqrt{1+r^2}}{k} & 0 \\ 0 & 0 & 0 & 1 \end{pmatrix}, \tag{2.18}$$

where $k^2 = 1 + r^2 + w^2$. In the rotated basis the mass-squared matrix has the form

$$\tilde{M}^2 = \left(\tilde{M}^{2\,(0)} v_R^2 + \tilde{M}^{2\,(1)} v_R + \tilde{M}^{2\,(2)}\right). \tag{2.19}$$

It is straight forward to check that both $\tilde{M}^{2\,(0)}$ and $\tilde{M}^{2\,(1)}$ have one zero eigenvalue. The positivity of the non-zero eigenvalues of $\tilde{M}^{2\,(0)}$ leads to the following constraints on the quartic couplings

$$2\rho_{12} = \rho_2 - 2\rho_1 > 0 \quad \text{and} \quad \alpha_{34} = \alpha_3 - \alpha_4 > 0\,. \tag{2.20}$$

Using non-degenerate perturbation theory, the smallest eigenvalue of M^2, which we take to be Higgs boson mass m_h^2, is found to be

$$\begin{aligned} m_h^2 &= (\tilde{M}^{2\,(2)})_{11} - \frac{[(\tilde{M}^{2\,(1)})_{14}]^2}{2\rho_1} \\ &= \frac{\kappa_1^2}{2(1+r^2+w^2)} \\ &\quad \times \Bigg(4\Big(\lambda_1(r^2+1)^2 + 4r(\lambda_4(r^2+1) + r\lambda_{23}) + w^2(\alpha_{124} + r^2(\alpha_1+\alpha_3) + \alpha_2 r) + \rho_1 w^4\Big) \\ &\qquad - \frac{1}{\rho_1}(\alpha_{124} + r^2(\alpha_1+\alpha_3) + \alpha_2 r + 2\rho_1 w^2)^2 \Bigg), \end{aligned} \tag{2.21}$$

where $\alpha_{124} = \alpha_1 + r\alpha_2 + \alpha_4$ [11]. Since m_h^2 should be positive, the second term in eq. (2.21) must always be less than the first. Thus the Higgs mass constraint imposes a rather strong restriction on the quartic couplings of DLRSM.

JHEP03(2023)168

However, it has to be noted that for some specific set of values of quartic couplings, the assumptions of non-degenerate perturbation theory will not be valid. In these scenarios, the smallest eigenvalue of M^2 matrix may differ significantly from the value given by the expression in eq. (2.21). We are interested in exploring the constraints on full parameter space of the quartic couplings. Therefore, we diagonalize the mass matrix numerically to avoid the pitfalls of possible near degeneracies of the diagonal elements of M^2 matrix. As discussed in the introduction, we need a v_R of about 20 TeV to satisfy the experimental lower bound on heavy charged gauge boson mass. Hence, we set $v_R = 20\,\text{TeV}$ in our numerical work, which also ensures that $\kappa_1^2, \kappa_2^2, v_L^2 \ll v_R^2$.

DLRSM contains the following extra scalars compared to the SM:

- three CP-even scalars, labelled $H_{1,2,3}$ earlier in this section,
- two CP-odd scalars, labelled A_1 and A_2,
- two pairs of charged scalars, labelled $H_1^\pm$ and $H_2^\pm$.

Among these, the CP-even scalar H_3 has some peculiar properties. Its predominant component is the $\text{SU}(2)_R$ scalar χ_R^0 and its mass is given by $m_{H_3}^2 \approx 2\rho_1 v_R^2$. Its couplings to SM fermions and gauge bosons are highly suppressed. Hence mass constraints on neutral scalars from neither flavour changing neutral interactions (FCNI) nor direct searches are applicable to H_3. In principle, its mass can be quite low [13], much lower than those of H_1 and H_2. The rest of the extra scalars can have significant coupling to SM fermions and gauge bosons and hence all the experimental constraints on heavy scalar masses will be applicable to them.

The gauge and the mass eigenstates of the neutral scalars are related by

$$X_{\text{ph}} = U^T X, \qquad U^T M^2 U = M^{2\,\text{diag}}. \tag{2.22}$$

The coupling of scalars in the gauge basis to W_1 boson is

$$\mathcal{L} \supset \frac{1}{2} g^2 \left((\kappa_1 - 2c_\xi s_\xi \kappa_2)\phi_{1r}^0 + (\kappa_2 - 2c_\xi s_\xi \kappa_1)\phi_{2r}^0 + v_L c_\xi^2 \chi_{Lr}^0 + v_R s_\xi^2 \chi_{Rr}^0 \right) W_{1\mu}^+ W_1^{-\mu}, \tag{2.23}$$

where ξ is the mixing angle between $W_{L,R}$ given by eq. (2.9). Transforming the scalar gauge eigenstates to mass eigenstates, we find the coupling multiplier for the 3-point interaction of h to W_1 bosons to be

$$\kappa_W = \frac{c_{hW_1W_1}}{c_{hWW}^{\text{SM}}} = \frac{1}{k}\left((1 - 2c_\xi s_\xi r)U_{11} + (r - 2c_\xi s_\xi)U_{21} + w c_\xi^2 U_{31} + \frac{v_R}{\kappa_1} s_\xi^2 U_{41} \right), \tag{2.24}$$

where we expressed the DLRSM coupling in the form of a ratio to the corresponding SM coupling. This makes is easier to compare our model calculations with the experimental results of Higgs boson couplings because they are given in the form of such ratios. Similarly, the coupling of scalars in gauge basis to the Z_1-boson is

$$\mathcal{L} \supset \frac{g^2}{4} (c_W + s_W s_Y)^2 (\kappa_1 \phi_{1r}^0 + \kappa_2 \phi_{2r}^0 + v_L \chi_{Lr}^0)\, Z_{1\mu}\, Z_1^\mu, \tag{2.25}$$

JHEP03(2023)168

which gives

$$\kappa_Z = \frac{g^2(g^2+2g_{BL}^2)}{(g^2+g'^2)(g^2+g_{BL}^2)}\,\frac{1}{k}\,(U_{11}+rU_{21}+wU_{31})\,. \tag{2.26}$$

Here g' is the gauge coupling of $\mathrm{U}(1)_Y$ of SM. We use $g_{BL} = gg'/(g^2-g'^2)^{1/2}$ which reduces the fraction involving the gauge couplings in eq. (2.26) to unity [17].

Triple Higgs (h^3) vertex in this model is given by

$$\begin{aligned} c_{h^3} = \frac{\kappa_1}{2}\Big(&2(\lambda_1+r\lambda_4)U_{11}^3+2(r\lambda_1+\lambda_4)U_{21}^3+2w\rho_1U_{31}^3+2(r(\lambda_1+4\lambda_2+2\lambda_3)+3\lambda_4)U_{11}^2U_{21}\\ &+2(\lambda_1+4\lambda_2+2\lambda_3+3\lambda_4 r)U_{11}U_{21}^2+w(\alpha_1+\alpha_4)U_{11}^2U_{31}+(\alpha_1+r\alpha_2+\alpha_4)U_{11}U_{31}^2\\ &+w(\alpha_1+\alpha_3)U_{21}^2U_{31}+(\alpha_2+r(\alpha_1+\alpha_3))U_{21}U_{31}^2\Big)\,, \end{aligned} \tag{2.27}$$

with the corresponding coupling multiplier being $\kappa_h = c_{h^3}/c_{h^3}^{\mathrm{SM}}$ where $c_{h^3}^{\mathrm{SM}} = m_h^2/2v$.

2.4 The fermion sector

The fermions obtain masses through their Yukawa couplings to the bidoublet. For the quark sector, these couplings are

$$\mathcal{L}_{\mathrm{Yuk}} \supset -\bar{Q}_{Li}(y_{ij}\Phi+\tilde{y}_{ij}\tilde{\Phi})Q_{Rj}+h.c.\,, \tag{2.28}$$

which lead to the following mass terms

$$\mathcal{L}_m \supset -\bar{U}'_{Li}(M_U)_{ij}U'_{Rj}-\bar{D}'_{Li}(M_D)_{ij}D'_{Rj}+h.c.\,. \tag{2.29}$$

Here $U' \equiv (u',c',t')$ and $D' \equiv (d',s',b')$ are up- and down-type quarks in the gauge basis. The mass matrices $M_{U(D)}$, in general, are complex and arbitrary

$$M_U = \frac{1}{\sqrt{2}}(\kappa_1 y+\kappa_2\tilde{y}),\quad M_D = \frac{1}{\sqrt{2}}(\kappa_2 y+\kappa_1\tilde{y})\,.$$

They must be diagonalized to identify the quark mass eigenstates. Interactions of the gauge eigenstates of the neutral CP-even scalars to quarks are given by [18]

$$\begin{aligned} \mathcal{L}_N \supset\ &\frac{\kappa_1}{\sqrt{2}\,\kappa_-^2}\,\bar{u}_{Li}\Big((\phi_1^0-r\phi_2^{0*})\hat{M}_u+(-r\phi_1^0+\phi_2^{0*})V_L^{\mathrm{CKM}}\,\hat{M}_d\,V_R^{\mathrm{CKM}\dagger}\Big)u_{Rj}\\ &+\frac{\kappa_1}{\sqrt{2}\,\kappa_-^2}\,\bar{d}_{Li}\Big((\phi_1^{0*}-r\phi_2^0)\hat{M}_d+(-r\phi_1^{0*}+\phi_2^0)V_L^{\mathrm{CKM}\dagger}\,\hat{M}_u\,V_R^{\mathrm{CKM}}\Big)d_{Rj}+h.c.\,, \end{aligned} \tag{2.30}$$

where $\kappa_-^2 = \kappa_1^2-\kappa_2^2 = (1-r^2)\kappa_1^2$ and $\hat{M}_{u(d)}$ is the diagonal up (down)-type quark matrix.[1] As we consider a scalar sector that conserves CP at the tree-level, manifest left-right symmetry holds in the quark sector, i.e., $V_R^{\mathrm{CKM}} = V_L^{\mathrm{CKM}}$. We use the Wolfenstein parametrization of the CKM matrix with best-fit values of relevant parameters [19]

$$A = 0.79,\ \ \lambda = 0.2265,\ \ \bar{\rho} = 0.141,\ \ \bar{\eta} = 0.357\,.$$

[1] In the gauge basis of the scalars, the Yukawa sector of DLRSM is the same as a triplet left-right symmetric model of ref. [18].

JHEP03(2023)168

Using eqs. (2.22) and (2.30) we obtain the couplings of CP-even scalars with quarks. We find that the couplings of fermions to the lightest scalar h are essentially flavour diagonal with small flavour violating couplings of the order of v^2/v_R^2. The heavier scalars, with masses of the order of v_R, have flavour violating couplings in general. For $v_R = 20\,\text{TeV}$, the amplitudes of FCNI are below the experimental upper bounds. The coupling of the CP-even lightest scalar to third generation quarks are given as

$$c_{htt\,(hbb)} = \frac{\kappa_1}{\sqrt{2}\,\kappa_-^2}\left((U_{11} - rU_{21})m_{t(b)} + (U_{21} - rU_{11})(V_L^{\text{CKM}}\,\hat{M}_{d(u)}\,V_R^{\text{CKM}\dagger})_{33}\right), \tag{2.31}$$

which can be used to obtain the coupling multipliers κ_t and κ_b, as $\kappa_f = c_{hff}/c_{hff}^{\text{SM}}$, where $c_{hff}^{\text{SM}} = m_f/v$ and $f = t$ or b.

3 Theoretical constraints

Here we briefly discuss the theoretical constraints on DLRSM, such as perturbativity of the quartic and Yukawa couplings, perturbative unitarity of gauge boson scattering, and boundedness of the scalar potential from below.

3.1 Perturbativity of the quartic and Yukawa couplings

Perturbativity bounds on the quadratic couplings dictate $\alpha_i, \lambda_i, \rho_j \lesssim 4\pi$, where $i = 1, 2, 3, 4$ and $j = 1, 2$. Moreover, we also assume $\mu_4 \lesssim v_R$.

Perturbativity of the Yukawa couplings y and $\tilde{y}$ appearing in eq. (2.28) pose a strong bound on the $r - w$ plane. In the limit $\left(V_{L,R}^{\text{CKM}}\right)_{33} \sim 1$,

$$\begin{aligned} y_{33} &= \frac{\sqrt{2}(1 + r^2 + w^2)^{1/2}}{v(1 - r^2)}\,(m_t - r\,m_b)\,, \\ \tilde{y}_{33} &= \frac{\sqrt{2}(1 + r^2 + w^2)^{1/2}}{v(1 - r^2)}\,(m_b - r\,m_t)\,. \end{aligned} \tag{3.1}$$

From these equations, we note that $y_{33} \simeq 1$ and $\tilde{y}_{33} \simeq 1/40$ for very small values of r and w. The perturbativity requirement of $y_{33} < (4\pi)^{1/2}$ leads to strong upper limits $r \lesssim 0.8$, and $w \lesssim 3.5$. The perturbativity requirement of $\tilde{y}_{33}$ gives comparatively weaker constraints. These constraints are shown in figure 1.

3.2 Perturbative unitarity of gauge boson scattering

The condition of unitarity of the $2 \to 2$ scattering of the gauge degrees of freedom impose certain constraints on the masses and couplings of the new scalars. Some of these constraints are superseded by perturbativity for $r < 1$. But the following conditions must be satisfied

JHEP03(2023)168

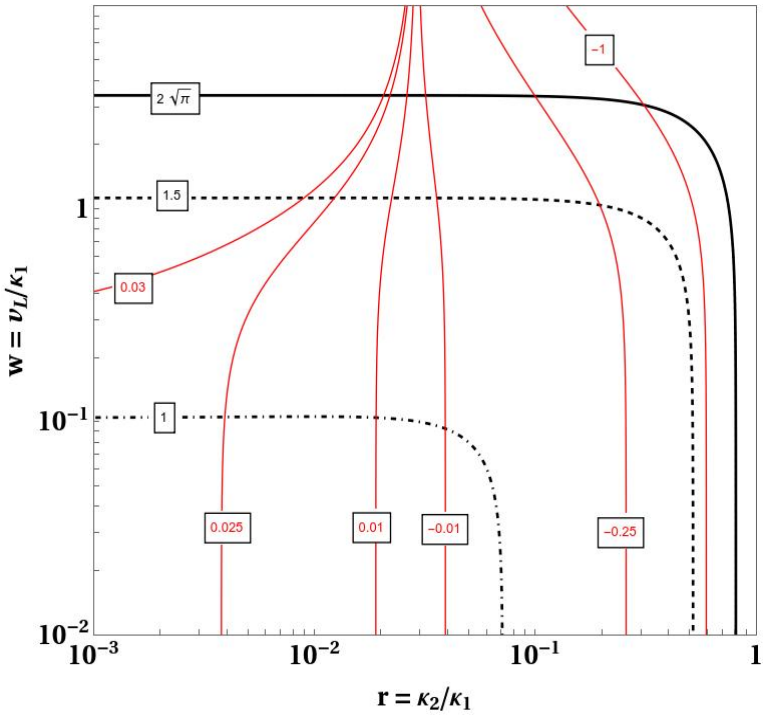

Figure 1. The black and red contours represent the values of y_{33} and $\tilde{y}_{33}$ respectively.

at $\mathcal{O}(\kappa_1/v_R)$ [11]

$$
\begin{aligned}
0 < \rho_1 < \frac{8\pi}{3}\,, \text{ or, } \frac{m_{H_3}^2}{v_R^2} < \frac{16\pi}{3}\,,\\
\frac{(c_{H_3})^2}{k^4}\,\frac{m_{H_3}^2}{v_R^2} < \frac{16\pi}{3}\,,\\
2\frac{w^2}{k^2}\sum_{i=1,2} F_i^2\frac{m_{H_i^\pm}^2}{v_R^2} + \frac{c_{H_3}}{k^2}\frac{m_{H_3}^2}{v_R^2} < 16\pi\,,\\
2\frac{w^2}{k^2}\sum_{i=1,2} S_i^2\frac{m_{H_i^\pm}^2}{v_R^2} + \frac{c_{H_3}}{k^2}\frac{m_{H_3}^2}{v_R^2} < 16\pi\,,
\end{aligned}
\tag{3.2}
$$

where the expressions for c_{H_3}, S_i and F_i, in terms of the parameters of the Higgs potential, are given in ref. [11].

3.3 Boundedness from below

Criteria for boundedness from below of the DLRSM scalar potential has been studied in the literature utilising the copositivity criteria [20, 21] and gauge orbit formulation [22–24]. These studies used different simplified forms of the potential. We have derived the criteria for boundedness from below for the most general potential given by eq. (2.3). These are described in appendix B.

JHEP03(2023)168

3.4 Custodial symmetry breaking

Some key constraints on the extended scalar sectors arise from the measurement of the ρ parameter, which quantifies the breaking of the custodial symmetry of the scalar potential in the SM. The tree-level contribution to $\rho = m_{W_1}^2/m_{Z_1}^2 \cos\theta_W^2$ in the DLRSM appears at the order $(v/v_R)^2$ [11].

4 A convenient parametrization of the quartic couplings

The model contains ten quartic couplings overall, four λs, four αs and two ρs. These couplings have to satisfy various inequalities arising from the theoretical constraints discussed in the previous section and the positivity of CP-even scalar masses. There is an inequality on the ratio $x = \lambda_2/\lambda_4$ arising from boundedness of the scalar potential. As shown in appendix B, this inequality is of the form $8x(1-x) > 0$. For positive x, this translates into $0.25 \leq x \leq 0.85$.

We are interested in how the Higgs data constrain ranges of r and w. In studying these constraints, in principle, the ten quartic couplings should be allowed to take ten independent values, subject to the inequalities mentioned above. However, a study with ten free parameters does not give a good insight into various inter-relations. To gain an insight as to how the data constrains r and w, we pick a simplified set of three quartic couplings λ_0, α_0 and ρ_1. We fix the ten quartic couplings by using relations

$$\left\{\lambda_1 = \lambda_3 = \lambda_4 = \lambda_0,\ \ x = \frac{\lambda_2}{\lambda_4},\ \ \alpha_1 = \alpha_2 = \alpha_4 = \alpha_0,\ \ p = \frac{\alpha_3}{\alpha_4} - 1,\ \ q = \frac{\rho_2}{2\rho_1} - 1\right\}. \quad (4.1)$$

The set of parameters $\{\lambda_0, \alpha_0, \rho_1, x, p, q, r, w, v_R\}$ together with v provides the most minimal simplified basis to describe the scalar potential of the model. From now on we refer to this as the '*simple*' basis, as opposed to the '*generic*' basis where all the λs and all the αs are taken to be independent. We note that, both in the simple basis and in the generic basis, p and q parameters need to be positive.

5 Constraints from the Higgs data

In section 3, we derived the upper bounds on r and w from theoretical constraints. In this section, we investigate the constraints on these parameters coming from the Higgs data. We first do this study in the *simple* basis of the DLRSM quartic couplings to see the pattern of allowed regions in the $r - w$ plane. We then re-do the study in the *generic* basis to see what changes, if any, are there in our results.

5.1 Constraints in the *simple* basis

In the *simple* basis, there are eight parameters, three quartic couplings, the three ratios p, q and x, the coupling of three scalar multiplets μ_4, and v_R. In our calculations, we fix the values of $v_R = 20\,\text{TeV}$. We vary the other parameters randomly and identify regions in the parameter space which satisfy the experimental constraints from the Higgs data.

JHEP03(2023)168

Observable	Observed value
m_h	(125.38 ± 0.14) GeV [25]
κ_W	1.05 ± 0.06 [26]
κ_Z	0.96 ± 0.07 [27]
κ_h	$[-2.3, 10.3]$ at 95% CL [28]
κ_t	1.01 ± 0.11 [27]
κ_b	$0.98^{+0.14}_{-0.13}$ [26]

Table 1. Experimental values of the Higgs mass and coupling multipliers used in our calculations.

The mass of the lightest Higgs scalar depends strongly on the quartic couplings λ, as shown in eq. (2.21). Hence, the constraint on m_h will be satisfied only for a limited range of values of λ_0. Therefore, in choosing random values of this parameter, we limit ourselves to a restricted range. For specific values of α_0, ρ_1, x, p, and q, we solve eq. (2.21) and obtain a solution for λ_0 which we label Λ_0. To maximize the number of points satisfying the m_h constraint, we choose random values of λ_0 in the limited range

$$\lambda_0 = (1 + y)\,\Lambda_0 \text{ with } y \in [-0.1, 0.1]. \tag{5.1}$$

This choice ensures that most of the random points satisfy the Higgs mass constraint and enables us to study how the constraints from the κ factors restrict the parameters of the model.

The random values of x and y are picked in linear scale in their respective ranges. For the other parameters, the random values are picked in a log scale, in the ranges specified below:

$$\alpha_{1,2,4} \equiv \alpha_0 \in [10^{-3}, 4\pi],\ \rho_1 \in [0.1, 8\pi/3],\ \mu_4 \in [10^{-2}, 1] \times v_R. \tag{5.2}$$

This choice of using logarithmic scale, leads to very small values of the parameters being as likely as the values of the order 1. Of the two ratios, p and q, we hold q fixed at $q = 1$ but consider four different values for p, varying from a low value of 0.02 to a high value of 5.

For each random point, we numerically calculate the lightest Higgs mass m_h and the coupling parameters κ_W, κ_Z, κ_h, κ_t and κ_b and demand that they should match the corresponding experimentally measured values, listed in table 1. The results of our calculation are displayed in figure 2. The light blue dots satisfy the theoretical bounds and the constraints from m_h, κ_h, κ_W, κ_Z and κ_t. By considering these constraints individually, it was found the κ_h constraint rules out a significant number of points allowed by the m_h constraint. The κ_W, κ_Z and κ_t constraints are satisfied by all the points which satisfy m_h and κ_h constraints. The red dots satisfy the additional constraint from κ_b parameter. The κ_b constraint leads to a drastic reduction in the number of allowed points for low values of p. In particular, for $p = 0.02$, very low values of r and w are ruled out. As the value of p increases, points of low r and low w become allowed but there is a clear preference for larger values of w as long as $p \leq 0.1$. Only for $p \geq 1$, the distribution of allowed points is uniform over the full range of r and w. This means we need to have α_3 at least twice as large as the other α s, if the usual assumption $v_L, \kappa_2 \ll \kappa_1$ is to hold.

JHEP03(2023)168

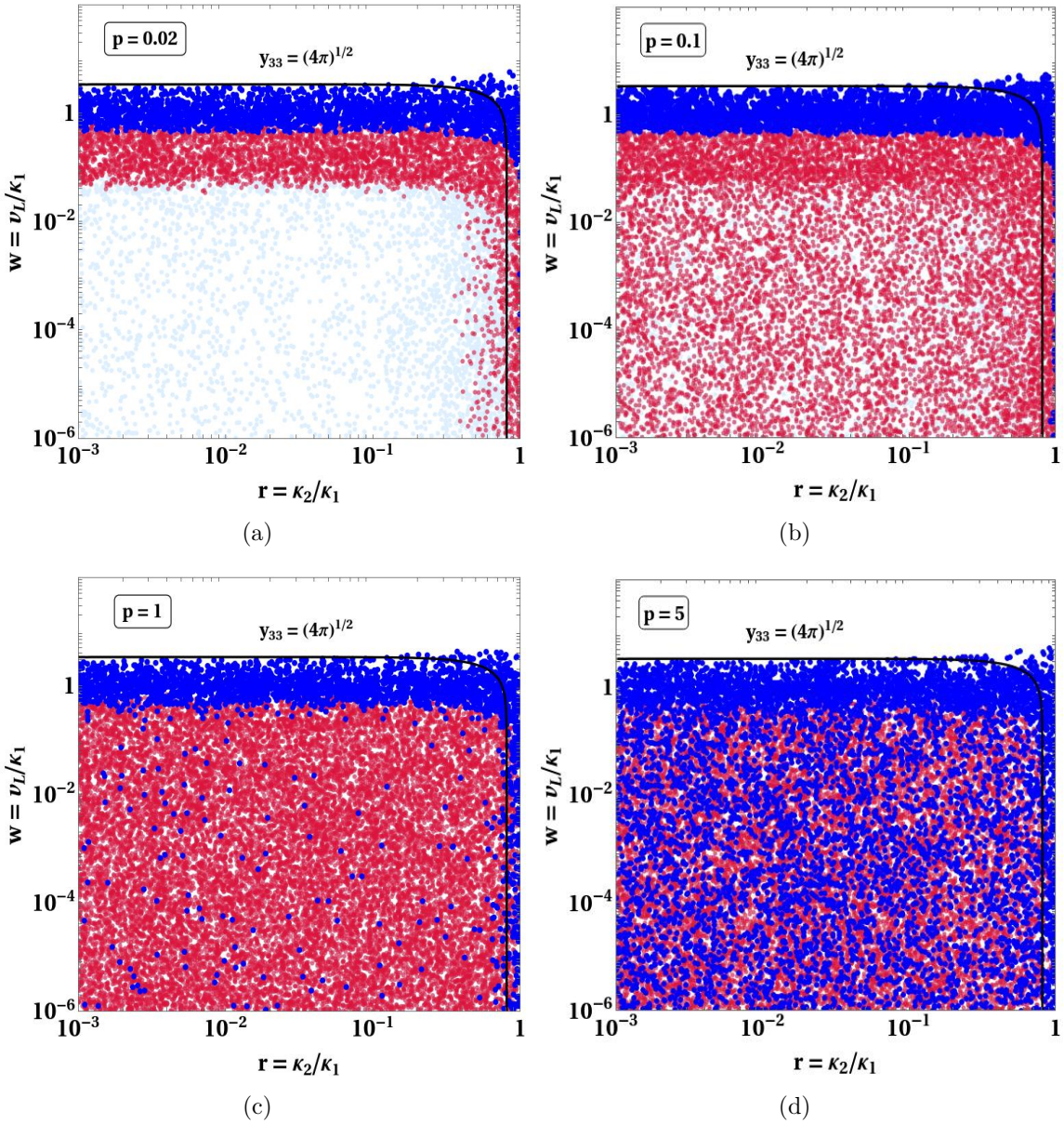

Figure 2. Allowed points on the r-w plane with random values of $\alpha_{1,2,4} = \alpha_0 \in [10^{-3}, 4\pi]$, $\lambda_{1,3,4} = \lambda_0 \in [10^{-3}, 4\pi]$, $x = \lambda_2/\lambda_0 \in [0.25, 0.85]$, $\rho_1 \in [0.1, 4\pi]$ for four different values of p. The values of q and v_R are held fixed at $q = 1$ and $v_R = 20\,\text{TeV}$ respectively. Light blue points satisfy m_h, κ_h, κ_W, κ_Z and κ_t constraints and theoretical bounds. Red points satisfy κ_b constraint also and dark blue points satisfy the additional constraint $m_{H_1} > 15\,\text{TeV}$.

The reason for this strong influence of κ_b can be understood from eqs. (2.17) and (2.31). In the expression for κ_b in eq. (2.31), the second term is proportional to m_t. If the CP-even scalar mixing matrix element U_{21} is not negligible, this second term can lead to a large value of κ_b. The dominant contribution to $m^2_{H_1}$ comes from $v_R^2 M_{22}^{2(0)} = v_R^2\,[p\,\alpha_3 + 2w^2\rho_{12}]/[2(1-r^2)]$ in eq. (2.17). If $M_{22}^{2(0)}$ is too small, there will be a significant mixing between h and H_1, i.e., U_{21} is not negligible and the predicted κ_b will deviate significantly from 1. A large value for

JHEP03(2023)168

$M_{22}^{2(0)}$ can be obtained for $r \simeq 1$, independent of the values of p and w, but this violates the perturbativity of the Yukawa coupling y_{33} and is not allowed. For moderate values of r, either p or w (or both) must take reasonably large values to satisfy the constraint on κ_b. We see this feature illustrated in figure 2 where small values of w are ruled out by the κ_b constraint when p is small but become progressively more allowed as p becomes larger.

In addition to the constraint from the measured parameters listed in table 1, there is an important indirect bound on the masses of heavy CP-even scalars from flavour changing neutral interactions. The requirement that these interactions be adequately suppressed leads to a strong bound [29]

$$m_{H_1} \geq 15\,\text{TeV}. \tag{5.3}$$

In figure 2, dark blue dots represent the points which satisfy this additional constraint also. For $p \leq 1$, the blue dots are bunched towards values of $w \geq 0.6$. The few points of low w, which occur for $r \simeq 1$ are ruled out by the constraint $r \leq 0.8$, arising from the perturbativity bound on the Yukawa coupling y_{33}. Therefore, the bound on m_{H_1} strongly prefers that *vev* of χ_L has a significant influence on the breaking of $\text{SU}(2)_L$. For very large values of $p \geq 5$, we see a reasonably large number of blue dots in the region of low r and low w. For example, in figure 2 (d), the range $r \in [10^{-3}, 10^{-2}]$ and $w \in [10^{-6}, 10^{-3}]$ contains $\sim 14\%$ of the total number of points allowed from the measurements of m_h, κ_h, κ_t, κ_b, and $m_{H_1} > 15\,\text{TeV}$. These points correspond to larger values of $\rho_1 \gtrsim 1$ which push $\rho_2 > 4$ making it relatively large. That is, the usual assumption $v_L, \kappa_2 \ll \kappa_1$ holds, only if the quartic couplings ρ_1 and ρ_2 take moderately large values.

In the expression for κ_h in eq. (2.27), the terms proportional to w always make a positive contribution to the value of κ_h. Hence, the experimental upper limit on κ_h affects the region of large w significantly. In future, if this upper limit is improved to $\kappa_h < 2$, values of $w > 1$ will be ruled out. Hence the points satisfying all the constraints (dark blue points of figure 2) will occur only for very large values of $p \sim 5$ with allowed values of $w < 0.5$.

We now briefly discuss what happens when the ratio q is allowed to deviate from 1. From eq. (2.17), we see that leading contribution to the mass of one of the heavier Higgses is $\rho_{12} v_R^2 = \rho_1 q v_R^2$. Hence, very small values of q will not satisfy $m_{H_1} > 15\,\text{TeV}$ constraint whereas larger values of q will violate unitarity bounds. These two constraints together restrict q to the range $0.01 \leq q \leq 4$. The constraints from m_h, κ_h, κ_W, κ_Z, κ_t and κ_b are unaffected by changes in the value of q. As a result, the points satisfying all the constraints (dark blue points of figure 2) are depleted overall if q deviates from 1. For the extreme allowed values of q, i.e., $q \sim 0.01$ and $q \sim 4$, $m_{H_1} > 15\,\text{TeV}$ is more likely to be satisfied for $w \gtrsim 1$. As mentioned above, these extreme values will be ruled out if κ_h is measured to be less than 2.

In the analysis above, the constraints on m_h and m_{H_1} were discussed thoroughly. Here we briefly comment on the masses of the additional scalars in the model. The algebraic expressions for their masses are given in appendix A. We find that m_{H_1}, m_{A_1} and $m_{H_1^\pm}$ are all highly degenerate with their masses differing by less than 1%, for the values of quartic couplings which satisfy all the experimental constraint listed in table 1. We also find that

JHEP03(2023)168

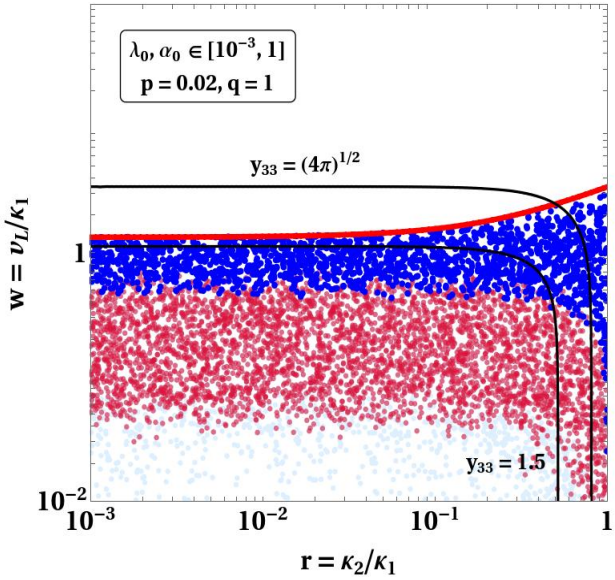

Figure 3. Allowed points on the r-w plane for $\lambda_i, \alpha_i \in [10^{-3}, 1]$, $\rho_1 \in [0.1, 8\pi/3]$, and $\rho_2 \in [0.1, 4\pi]$. The light blue points satisfy m_h, κ_W, κ_Z, κ_h and κ_t constraints and theoretical bounds. The red points satisfy κ_b constraint in addition and the dark blue points satisfy $m_{H_1} > 15\,\text{TeV}$ constraint. All the allowed points are below the red line, which represents the analytical upper limit of w. The black solid lines represent contours of Yukawa couplings y_{33}.

the masses of other scalars, m_{H_2}, m_{A_2} and $m^{\pm}_{H_2}$ are similarly degenerate but at a higher values compared to m_{H_1}.

5.2 A strong upper limit on v_L from Higgs mass

As mentioned earlier, the parameter space with $w \gtrsim 1$ is of special interest. It was seen in figure 2 that there is a strong upper bound on w arising from the measurement of m_h. In the *simple* basis eq. (2.21) takes the form

$$m_h^2 = \frac{v^2}{(1+r^2+w^2)^2}\left[2(8\lambda_2 r^2 + \lambda_0(1+r^2)^4) - \frac{\alpha_0^2(2+r(2+(2+p)r))^2}{2\rho_1}\right]. \tag{5.4}$$

In the limit $\alpha_0 \to 0$ and $r \to 1$, imposing the perturbativity bounds $\lambda_0, \lambda_2 < 4\pi$ leads to the upper limit $w < 6.81$. Demand of boundedness from below requires $\lambda_2 < 0.85\,\lambda_0$, which in turn, slightly reduces the upper limit to $w < 6.71$. The upper limit can also be obtained as a function of r, $w_{\max}(r) \simeq a + br + cr^2$, where $a = 2.9332$, $b = 4.3535$, and $c = -0.4755$. If the maximum values of the couplings α_0 and $\lambda_{0,2}$ are taken to be 1 instead of 4π, the upper limit reduces to $w_{\max} \sim 2.8$ at $r \sim 1$. In figure 3 we have illustrated this analytical bound on top of a random scan over $\alpha_0, \lambda_0 \in [10^{-3}, 1]$ which shows that all the allowed points are below the limit imposed by the Higgs mass constraint of eq. (5.4). Note that, the perturbativity limit on y_{33} is stronger than the Higgs data for $r \gtrsim 0.5$. As a result, the effective upper limit on w as a function of r is set by the interplay of m_h and perturbativity of y_{33}.

JHEP03(2023)168

5.3 Constraints in the *generic* basis

In the *generic* basis, each quartic coupling is allowed to take a different value. The total number of parameters in this case is eleven: ten quartic couplings (four α s, four λ s and two ρ s) and μ_4. As in the *simple* case, we parametrize $\alpha_3 = \alpha_4(1+p)$ and $\rho_2 = 2\rho_1(1+q)$. Random values of these quartic couplings are varied over the ranges

$$\lambda_2, \lambda_3, \lambda_4 \in [10^{-3}, 4\pi],\ \alpha_1, \alpha_2, \alpha_4 \in [10^{-3}, 4\pi],\ \rho_1 \in [0.1, 8\pi/3]. \tag{5.5}$$

As before, these random values are picked in a log scale. As in the *simple* case, to maximize the number of points satisfying the m_h constraint we choose random values of λ_1 in the limited range

$$\lambda_1 = (1+y)\,\Lambda_1 \text{ with } y \in [-0.1, 0.1], \tag{5.6}$$

where Λ_1 is the solution for λ_1 obtained by solving eq. (2.21) for a specific set of values of $\lambda_{2,3,4}$, $\alpha_{1,2,4}$, ρ_1, and p. The random values of y were chosen on a linear scale. The numerical calculations here also are done for $v_R = 20\,\text{TeV}$ and for four different values of p varying from 0.02 to 5. The value of q, as before, is fixed at $q = 1$.

The result of this scan can be seen in figure 4 for the four different values of p. As in the case of the *simple* basis, we have

- the light blue points satisfying the theoretical bounds and constraints from m_h, κ_h, κ_W, κ_Z, and κ_t,
- the red points satisfying the additional constraint from κ_b,
- the dark blue points satisfying the constraint from the lower limit on the heavy Higgs mass.

We note that the patterns of allowed points as a function of w, observed in figure 2 are repeated in figure 4. One contrast is that figure 4 contains very few allowed points at low values of r compared to figure 2. That is, if the quartic couplings are allowed to vary randomly without any pattern, it is more unlikely that r and w take very small values. Hence, for a generic set of values of quartic couplings in DLRSM, the probability that $\text{SU}(2)_L$ breaking occurs essentially due to the *vev* of ϕ_1^0 is very small. If such a feature is desired, then the quartic couplings should be fine-tuned to particular values.

5.4 Decoupling leads to alignment

In this subsection, we discuss the interplay of various constraints from the Higgs data on the allowed values of parameters. All the parameters of the model, including p and q, are varied in the ranges described previously in section 5.1 and in section 5.3. We have calculated the values of κ_b and κ_t for each of these points and plotted them in figure 5 in the $\kappa_b - \kappa_t$ plane.

The left panel of figure 5 is for the *simple* basis and the right panel is for the *generic* basis. The pink points satisfy the theoretical constraints. We note that all pink points satisfy the experimental constraint on κ_t but only a fraction of them satisfy the constraint on κ_b. The points which satisfy the constraints on m_h, κ_W, κ_Z, and κ_h form a small subset of pink points and are highlighted as blue points. We see that the κ_b constraint disallows

JHEP03(2023)168

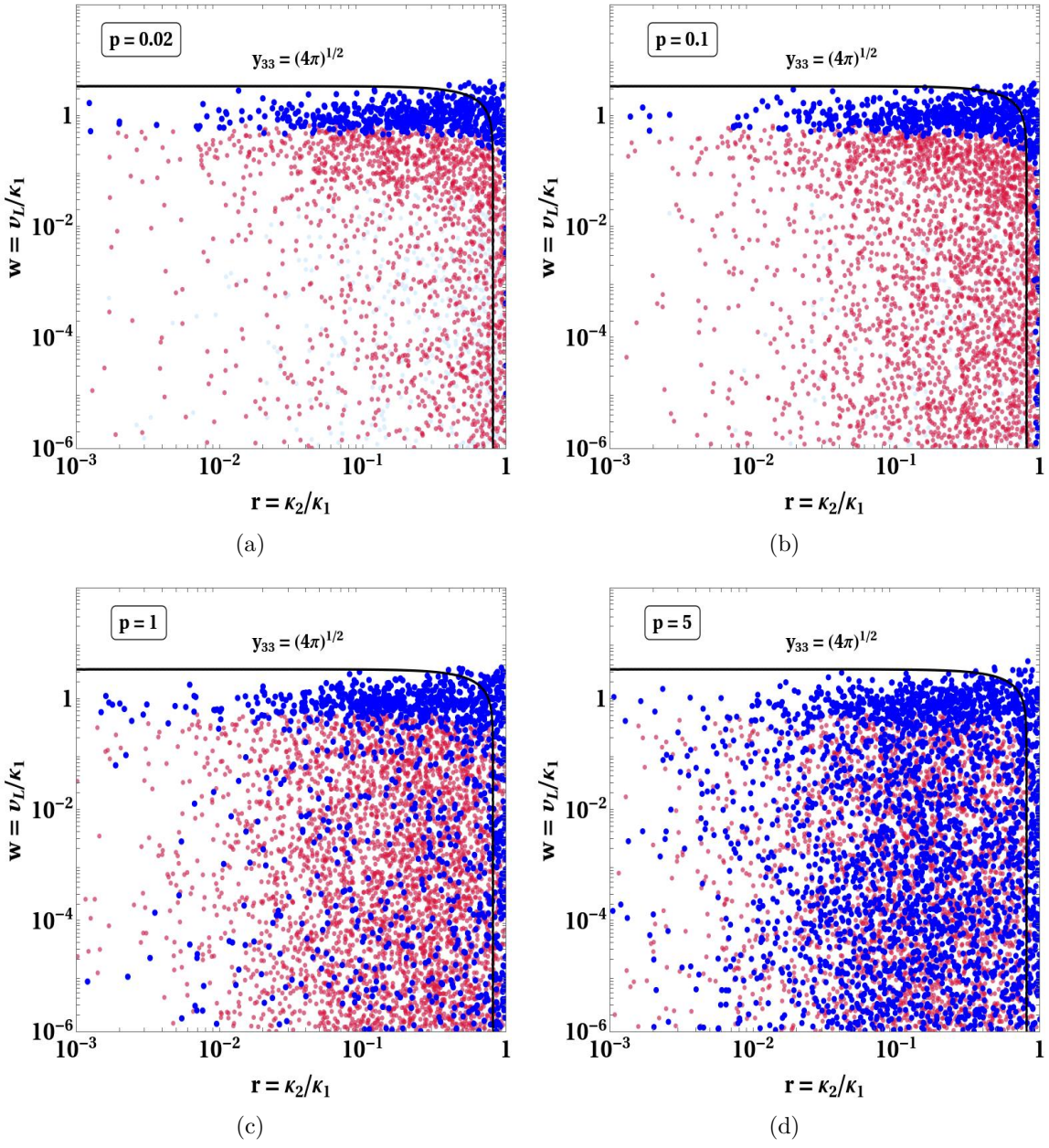

Figure 4. Allowed points on the r-w plane with random values of $\alpha_{1,2,4} \in [10^{-3}, 4\pi]$, $\lambda_{2,3,4} \in [10^{-3}, 4\pi]$, $\rho_1 \in [0.1, 8\pi/3]$, $q = 1$, while (a) $p = 0.02$, (b) $p = 0.1$, (c) $p = 1$, and (d) $p = 5$. The colour coding is the same as figure 2.

about 9% blue points. Finally, we impose the constraint on heavy Higgs mass $m_{H_1} > 15\,\text{TeV}$. The points which satisfy this last constraint are shown in dark green. These green points essentially form a very small fraction (2.5% of pink points) which are clustered around the point $\kappa_b = 1$ and $\kappa_t = 1$. This clustering around SM values of κ_b and κ_t is analogous to the scenario of 'alignment by decoupling' in two-Higgs-doublet model (2HDM) [30]. The Higgs sector of DLRSM effectively reduces to a special version of three-Higgs-doublet model at the electroweak scale, leading to this similarity with 2HDM.

JHEP03(2023)168

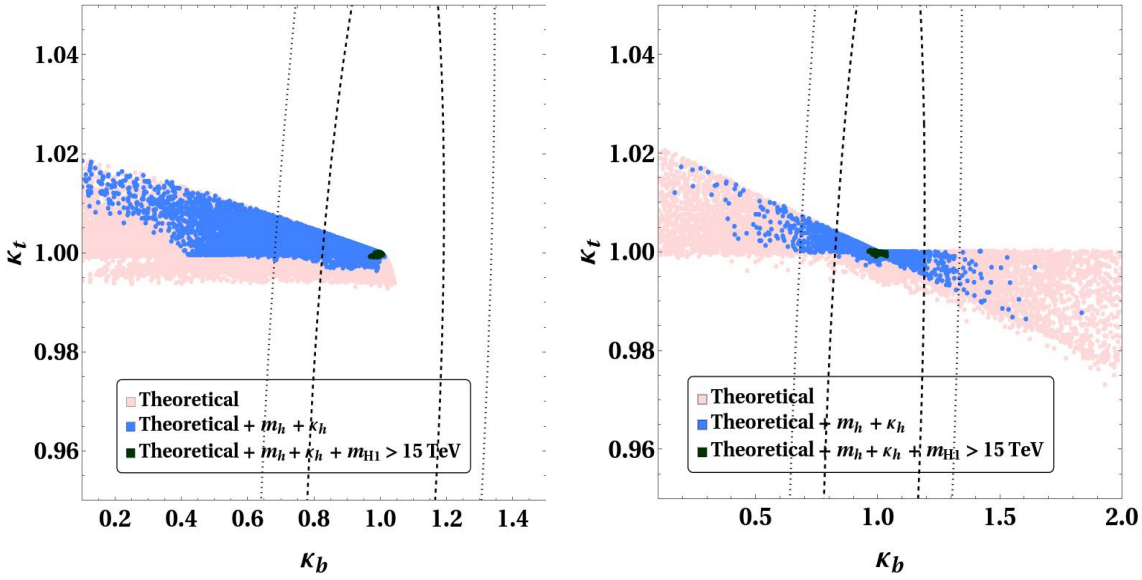

Figure 5. Predictions for κ_b and κ_t for (a) *simple* and (b) *generic* basis with random values of quartic couplings in the ranges given by eqs. (5.2) and (5.5) respectively. Additionally, p and q are varied logarithmically in the range $[0.1, 10]$. The pink points satisfy the theoretical constraints, the blue points satisfy the additional m_h and κ_h constraints, and dark green points also satisfy constraint on heavy Higgs mass $m_{H1} > 15\,\text{TeV}$.

6 Summary and outlook

We revisit the doublet left-right symmetric model with the scalar sector consisting of a bidoublet and two doublets. The two neutral scalars embedded in the bidoublet and the one from the $\text{SU}(2)_L$ doublet can all contribute to EWSB. The pattern of the EWSB in this model is parametrized by the two ratios of *vevs* $r = \kappa_2/\kappa_1$ and $w = v_L/\kappa_1$. Most studies of DLRSM take these two ratios to be very small. In this paper, we study how the Higgs data from LHC constrains these two parameters. In particular, we check the consistency of the usual assumption $r, w \ll 1$ with the data.

In our study, we demand that the parameters of our model should be such that

1. the Higgs potential is bounded from below,
2. the quartic couplings of the Higgs potential should satisfy perturbative unitarity,
3. the Yukawa couplings, particularly of third of generation of fermions, should be perturbative,
4. the mass-squared values of all CP-even Higgses should be positive.

The third condition in the above list leads to upper limits $r < 0.8$ and $w < 3.5$, whereas the fourth condition requires the two ratios of quartic couplings,

$$p = \frac{(\alpha_3 - \alpha_4)}{\alpha_4} \text{ and } q = \frac{(\rho_2 - 2\rho_1)}{2\rho_1},$$

JHEP03(2023)168

to be positive. We vary the parameters of the model, subject to the above constraints and study which values of parameters satisfy the experimental constraints on the lightest CP-even scalar mass m_h and its coupling to gauge bosons κ_W and κ_Z, its self-coupling κ_h, and its coupling to third generation quarks, κ_t and κ_b. We also imposed the additional constraint $m_{H_1} > 15\,\text{TeV}$.

The model contains ten quartic couplings. In order to get a better understanding of the interplay of different quartic couplings, we defined a simplified set of quartic couplings: the three quartic couplings λ_i, involving only the bidoublet Higgs Φ, are set equal λ_0 and three of the quartic couplings α_i, which couple the bidoublet to ordinary doublets χ_L and χ_R, are also set to equal to α_0. A fourth λ coupling is defined in terms of the ratio $x = \lambda_2/\lambda_4$, which is constrained to be in the range $0.25 \leq x \leq 0.85$ as shown in section 4. This *simple* set contains only six independent parameters, $\{\lambda_0, \alpha_0, \rho_1, x, p, q\}$.

We did our calculations first with the *simple* set of quartic couplings. We first fixed the value of the quartic coupling ratio $q = 1$ and considered four different values for the other quartic coupling ratio $p = 0.02, 0.1, 1, 5$. For these values of p and q, we picked a random set of values for the other parameters in their allowed ranges. For each random set, we computed $m_h, \kappa_W, \kappa_Z, \kappa_h, \kappa_t, \kappa_b$ and m_{H_1} and picked the points which satisfied the constraints on all the above quantities. We found that the points which satisfy the m_h constraint, typically satisfied the constraints from κ_W, κ_Z, and κ_t also. The κ_h constraint rules out a significant number of points allowed by m_h for large values of w. The constraint from κ_b has a non-trivial effect on the allowed points but the $m_{H_1} > 15\,\text{TeV}$ constraint rules out most of the points with low values of w. For values of $p \leq 0.1$, there were no allowed points for $w \lesssim 0.6$. For $p > 1$, a few random points satisfy all the experimental constraints and have $r < 10^{-2}$ and $w < 10^{-3}$. The number of such points, with very small values of r and w, steadily increase with increasing value of p and form 14% of all the allowed random points when $p = 5$. We find that such points also require $\rho_1 > 1$. Hence, we can conclude that the usual assumption that $v_L, \kappa_2 \ll \kappa_1$ holds true for only a fine-tuned set of parameters, in particular for somewhat large values of the quartic couplings ρ_1 and ρ_2. This statement is true even when the value of q is moved away from 1.

We repeated the above calculations with the full, *generic* set of quartic couplings. The low density of allowed points for small values of r and w not only persists in this case but becomes even more pronounced. Hence, our main conclusion is the following: most of the studies of the DLRSM assume $\kappa_1 \approx v$, with other *vev*s being negligibly small. On the contrary, we have pointed out that large values of r and w are allowed by the Higgs data and preferred by the indirect bound on m_{H1}. We also note that all the points satisfying $m_{H_1} > 15\,\text{TeV}$ constraint, also satisfy $\kappa_{t,b} \sim 1$ to a very good precision. This confirms that the lightest scalar in DLRSM achieves alignment with the SM-like Higgs through the decoupling of the heavier scalars.

JHEP03(2023)168

Acknowledgments

S.K. would like to thank Tuhin S. Roy for valuable discussions. J.M. acknowledges the support of the Department of Science and Technology (DST) of the Government of India through grant no. SR/WOS-A/PM-6/2019(G). S.K. and S.U.S. thank Ministry of Education, Government of India, for financial support through Institute of Eminence funding.

A Heavy Higgs and gauge boson masses

In this section we present the expressions for the masses of the heavy scalars, and the masses and mixing of neutral gauge bosons.

(a) Masses of the heavier CP-even neutral Higgses are given by

$$m^2_{H_1,H_2} = \frac{1}{4y}(a_1 \mp b_1), \quad m^2_{H_3} = 2\rho_1 v_R^2. \tag{A.1}$$

Masses of the heavier CP-odd neutral Higgses, A_1^0 and A_2^0 and the heavier charged scalars are given by

$$m^2_{A_1^0,A_2^0} = \frac{1}{4y}(a_2 \mp b_2)\,, \quad m^2_{H_1^\pm,H_2^\pm} = \frac{1}{4y}(a_3 \mp b_3) \tag{A.2}$$

where

$$\begin{aligned}
x &= 1 + r^2, y = 1 - r^2,\\
a_1 &= v_R^2(x\alpha_{34} + 2\rho_{12}(2w^2 + y)),\\
a_2 &= v_R^2\Big(x\alpha_{34} + 2y\rho_{12} + 2w^2\rho_{12}\Big) + \kappa_1^2\Big(- 4xy\lambda_{23} + w^2(x\alpha_{34} + 2y\rho_{12})\Big),\\
a_3 &= v_R^2\Big(x\alpha_{34} + 2y\rho_{12} - 4w^2\rho_{12}\Big) + \kappa_1^2\Big(2y^2\alpha_{34} + xw^2(\alpha_{34} - 2\rho_{12})\Big),\\
b_1 &= v_R^2\left[\left(x\alpha_{34} + 2\rho_{12}\frac{r^4 + 4r^2w^2 - 1}{x}\right)^2 + 16\rho_{12}^2 r^2 w^2\frac{(x + w^2)y^2}{x^2}\right]^{1/2},\\
b_2 &= \Bigg[v_R^4\Big(x^2\alpha_{23}^2 + 4(4r^2w^2 - xy)\alpha_{34}\rho_{12} + (xy^2 + 16r^2w^2(w^2 - yr^2))\rho_{12}^2\Big)\\
&\quad + \kappa_1^4\Big(- 4xy\lambda_{23} + w^2(x\alpha_{34} - 2y\rho_{12})\Big)^2\\
&\quad + 2\kappa_1^2 v_R^2\Big(8r^2w^4\rho_{12}(\alpha_{34} - y\rho_{12}) - 4xy\lambda_{23}(x\alpha_{34} - 2y\rho_{12})\\
&\quad + w^2(x^2\alpha_{34}^2 - 4y(x\alpha_{34} + 8r^2\lambda_{23})\rho_{12} + 4y^2\rho_{12}^2)\Big)\Bigg]^{1/2},\\
b_3 &= \Bigg[w^4\kappa_1^4(x\alpha_{34} - 2y\rho_{12})^2 + 2v_R^2w^2\kappa_1^2\Big(\alpha_{34}^2(4r^2 - y^2) + 4(y^2 - 2r^2y + 2r^2w^2)\alpha_{34}\rho_{12}\\
&\quad - 4y(y^2 - r^2y + 2r^2w^2)\rho_{12}^2\Big)\\
&\quad + v_R^4\Big(x^2\alpha_{34}^2 + 4(4r^2w^2 - xy)\alpha_{34}\rho_{12} + 4(y^2 - 4r^2y + 4r^2w^4)\rho_{12}^2\Big)\Bigg]^{1/2},
\end{aligned} \tag{A.3}$$

JHEP03(2023)168

where α_{34}, λ_{23}, and ρ_{12} were previously defined. These expressions have been presented in the limit $\mu_4 = 0$.

(b) The massive neutral gauge bosons, Z_1^μ and Z_2^μ, and photon A^μ is expressed in terms of the unphysical fields as

$$
\begin{aligned}
A_\mu &= \frac{\tilde{g}}{g_L} W^3_{L\mu} + \frac{\tilde{g}}{g_R} W^3_{R\mu} + \frac{\tilde{g}}{g_{BL}} B_\mu, \\
Z_{1\mu} &= \frac{1}{D_1}\left(\frac{g_L(8m^2_{Z_1} - 2g_R^2 v_R^2)}{(g_R^2 v_R^2 - g_L^2 v_L^2)} W^3_{L\mu} + \frac{g_R(8m^2_{Z_2} - 2(g_L^2+g_R^2)\kappa_+^2 - 2g_R^2 v_R^2)}{(g_R^2 v_R^2 - g_L^2 v_L^2)} W^3_{R\mu} + 2g_{BL} B_\mu \right), \\
Z_{2\mu} &= \frac{1}{D_2}\left(\frac{-g_L(8m^2_{Z_2} - 2g_R v_R^2 - 2g_{BL}^2(v_L^2+v_R^2))}{(g_L^2 v_L^2 - g_R^2 v_R^2)} W^3_{L\mu} \right. \\
&\qquad \left. + \frac{g_R(8m^2_{Z_2} - 2g_L v_L^2 - 2g_{BL}^2(v_L^2+v_R^2)}{(g_L^2 v_L^2 - g_R^2 v_R^2)} W^3_{R\mu} + 2g_{BL} B_\mu \right),
\end{aligned}
\tag{A.4}
$$

where,

$$
\begin{aligned}
\frac{1}{\tilde{g}^2} &= \frac{1}{g_L^2} + \frac{1}{g_R^2} + \frac{1}{g_{BL}^2}, \\
D_1 &= \left[4g_{BL}^2 + \frac{1}{(g_L^2 v_L^2 - g_R^2 v_R^2)^2} \left(8m^2_{Z_2}(g_L^2+g_R^2) - 4g_L^2 g_R^2 \kappa_+^2 - 2g_L^4 v^2 - 2g_R^4 V^2 \right) \right]^{1/2}, \\
D_2 &= \left[4g_{BL}^2 + \frac{1}{(g_L^2 v_L^2 - g_R^2 v_R^2)^2} \left((g_L^2+g_R^2)(8m^2_{Z_2} - 2g_{BL}^2(v_L^2+v_R^2)) - 2g_L^2 g_R^2 (v_L^2+v_R^2) \right) \right]^{1/2}.
\end{aligned}
\tag{A.5}
$$

B Conditions for boundedness from below

In the presence of the most general doublet-bidoublet mixing, here we calculate the conditions for boundedness from below following the gauge orbit formulation of refs. [22, 31]. The unique form of the quartic term multiplied by α_2 prohibits any simple modification of existing bounds. The quartic potential of our interest is given by eq. (2.3). We choose the following parametrization:

$$
\begin{aligned}
&\mathrm{Tr}(\Phi^\dagger\Phi) + (\chi_L^\dagger \chi_L) + (\chi_R^\dagger \chi_R) \equiv R^2 \\
&\mathrm{Tr}(\tilde{\Phi}^\dagger\tilde{\Phi}) = \mathrm{Tr}(\Phi^\dagger\Phi) \equiv R^2 \cos^2\theta \\
&(\chi_L^\dagger \chi_L) \equiv R^2 \sin^2\theta \sin^2\gamma \\
&(\chi_R^\dagger \chi_R) \equiv R^2 \sin^2\theta \cos^2\gamma \\
&\mathrm{Tr}(\tilde{\Phi}^\dagger\Phi)/\mathrm{Tr}(\Phi^\dagger\Phi) \equiv \beta e^{-i\omega} \\
&\mathrm{Tr}(\Phi^\dagger\tilde{\Phi})/\mathrm{Tr}(\Phi^\dagger\Phi) \equiv \beta e^{i\omega} \\
&(\chi_L^\dagger \Phi\Phi^\dagger \chi_L)/\mathrm{Tr}(\Phi^\dagger\Phi)(\chi_L^\dagger\chi_L) \equiv \eta_1 \\
&(\chi_R^\dagger \Phi^\dagger\Phi \chi_R)/\mathrm{Tr}(\Phi^\dagger\Phi)(\chi_R^\dagger\chi_R) \equiv \eta_2 \\
&(\chi_L^\dagger \tilde{\Phi}\tilde{\Phi}^\dagger \chi_L)/\mathrm{Tr}(\tilde{\Phi}^\dagger\tilde{\Phi})(\chi_L^\dagger\chi_L) = \eta_3 \\
&(\chi_R^\dagger \tilde{\Phi}^\dagger\tilde{\Phi} \chi_R)/\mathrm{Tr}(\tilde{\Phi}^\dagger\tilde{\Phi})(\chi_R^\dagger\chi_R) = \eta_4,
\end{aligned}
$$

JHEP03(2023)168

where $R > 0$, $\{\theta, \gamma\} \in [0, \frac{\pi}{2}]$, $\beta \in [0, 1]$, and $\omega \in [0, 2\pi]$. The allowed range for these parameters is $\frac{1}{2}(1 - \sqrt{1-\beta^2}) < \eta_{1,2,3,4} < \frac{1}{2}(1 + \sqrt{1-\beta^2})$ along with

$$\eta_1 + \eta_3 = 1, \quad \eta_2 + \eta_4 = 1. \tag{B.1}$$

Using the parametric forms defined above we obtain

$$V_4 = R^4 \Big[\cos^4\theta\, f_1(\lambda_i, \beta, \omega) + \sin^4\theta\, f_2(\rho_i, \gamma) + \sin^2\theta \cos^2\theta\, f_3(\alpha_i, \gamma, \eta_i) \Big], \tag{B.2}$$

where

$$\begin{aligned} f_1(\lambda_i, \beta, \omega) &\equiv \frac{1}{4}(\lambda_1 + \lambda_2\beta^2 \cos 2\omega + \lambda_3\beta^2 + \lambda_4\beta\cos\omega), \\ f_2(\rho_i, \gamma) &\equiv \rho_1 \sin^4\gamma + \rho_1 \cos^4\gamma + \rho_2 \sin^2\gamma\cos^2\gamma, \\ f_3(\alpha_i, \gamma, \eta_i) &\equiv \alpha_1 + 2\alpha_2\beta\cos\omega + \alpha_3(\eta_1 \sin^2\gamma + \eta_2\cos^2\gamma) + \alpha_4(\eta_3\sin^2\gamma + \eta_4\cos^2\gamma). \end{aligned}$$

Upon applying the copositivity criteria, eq. (B.2) indicates that

$$f_1(\lambda_i, \beta, \omega) > 0, \tag{B.3}$$

$$f_2(\rho_i, \gamma) > 0, \tag{B.4}$$

$$f_3(\alpha_i, \gamma, \eta_i) + 2\sqrt{f_1(\lambda_i, \beta, \omega) f_2(\rho_i, \gamma)} > 0\,. \tag{B.5}$$

These conditions should hold for all possible values of the parameters $\{\beta, \omega, r, \eta_{1,2,3,4}, \gamma\}$.

- $f_1(\lambda_i, \beta, \omega)$ is minimized at $\beta = 0$, or $\sin\omega = 0$, and $\cos\omega = -\lambda_4/2\lambda_2$. Subsequently, certain combinations of λs can be obtained [22]

$$f_1 > 0 : \left\{ \begin{array}{ll} \lambda_1 & \\ \left(\lambda_1 - \frac{\lambda_4^2}{2\lambda_2+\lambda_3}\right) & \Longleftarrow\ 2\lambda_2 + \lambda_3 > |\lambda_4| \\ (\lambda_1 + \lambda_3 + 2(\lambda_2 - |\lambda_4|)) & \\ \left(\lambda_1 + \lambda_3 - 2\lambda_2 - \frac{\lambda_4^2}{4\lambda_2}\right) & \Longleftarrow\ |4\lambda_2| > |\lambda_4| \end{array} \right\} \tag{B.6}$$

  Here the notation "p $\Longleftarrow$ q" implies condition p has to checked if and only if condition q is true.

- $f_2(\rho_i, \gamma)$ is symmetric under the exchange $\sin\gamma \leftrightarrow \cos\gamma$. Thus f_2 becomes minimum at $\sin\gamma = \cos\gamma = \frac{1}{\sqrt{2}}$ and assumes the value $f_{2,\min} \equiv \frac{2\rho_1+\rho_2}{4}$. In the limits $\tan\gamma = 0$, and $\tan\gamma = \infty$, $f_{2,\min} = \rho_1$. This leads to the following boundedness criteria

$$f_2 > 0 : \quad \{\rho_1 > 0, \quad 2\rho_1 + \rho_2 > 0\}\,. \tag{B.7}$$

- Eq. (B.5) is symmetric under the exchange $\eta_1 \leftrightarrow \eta_2, \eta_3 \leftrightarrow \eta_4$, along with $\sin\gamma \leftrightarrow \cos\gamma$. The l.h.s. of eq. (B.5) thus takes a minimum value at $\eta_1 = \eta_2$, $\eta_3 = \eta_4$ and $\sin\gamma = \cos\gamma = \frac{1}{\sqrt{2}}$,

$$\alpha_1 + 2\alpha_2\beta\cos\omega + \alpha_3\eta_1 + \alpha_4\eta_3 + 2\sqrt{f_1(\lambda_i, \beta, \omega)\left(\frac{2\rho_1+\rho_2}{4}\right)} > 0 \tag{B.8}$$

JHEP03(2023)168

Eq. (B.1) implies that $\eta^{\rm min}_{1(2)} = \eta^{\rm max}_{3(4)}$ and vice versa. So third condition becomes

– for $\tan\gamma = 1$:

$$\alpha_1 + 2\alpha_2\beta\cos\omega + \frac{\alpha_3}{2}\left(1 \pm \sqrt{1-\beta^2}\right) + \frac{\alpha_4}{2}\left(1 \mp \sqrt{1-\beta^2}\right) + \sqrt{f_1(\lambda_i,\beta,\omega)\left(\frac{2\rho_1+\rho_2}{4}\right)} > 0, \tag{B.9}$$

– for $\tan\gamma = 0$ or $\tan\gamma = \infty$:

$$\alpha_1 + 2\alpha_2\beta\cos\omega + \frac{\alpha_3}{2}\left(1 \pm \sqrt{1-\beta^2}\right) + \frac{\alpha_4}{2}\left(1 \mp \sqrt{1-\beta^2}\right) + \sqrt{f_1(\lambda_i,\beta,\omega)\rho_1} > 0\,. \tag{B.10}$$

The contribution from α_2 dependent term of V_4 in eqs. (B.9) and (B.10) is given by $\tilde{f}_3(\alpha_2,\beta,\omega) = 2\alpha_2\beta\cos\omega$ which has a minimum value at $\beta = 0$ or $\sin\omega = 0$.

Case 1: For $\beta = 0$, $\tilde{f}_3(\alpha_2,\beta,\omega) = 0$.

Case 2: For $\sin\omega = 0$, $\cos\omega = \pm 1$, which implies $\tilde{f}_3(\alpha_2,\beta,\omega) = -2|\alpha_2|\beta$.

Case 3: On the boundary $\beta = 1$, $\tilde{f}_3(\alpha_2,\beta,\omega) = -2|\alpha_2|$.

Now we list the boundedness conditions emerging from eqs. (B.9) and (B.10) in the aforementioned limits.

- For $\beta = 0$,

$$\begin{aligned}
\alpha_1 + \alpha_3 + \sqrt{\lambda_1(2\rho_1+\rho_2)} &> 0\\
\alpha_1 + \alpha_4 + \sqrt{\lambda_1(2\rho_1+\rho_2)} &> 0\\
\alpha_1 + \alpha_3 + 2\sqrt{\lambda_1\rho_1} &> 0\\
\alpha_1 + \alpha_4 + 2\sqrt{\lambda_1\rho_1} &> 0\,.
\end{aligned} \tag{B.11}$$

- For $\sin\omega = 0$,

$$\begin{aligned}
&\alpha_1 - 2|\alpha_2|\frac{|\lambda_4|}{2\lambda_2+\lambda_3} + \frac{\alpha_3}{2}\left(1 \pm \sqrt{1-\frac{\lambda_4^2}{(2\lambda_2+\lambda_3)^2}}\right) + \frac{\alpha_4}{2}\left(1 \mp \sqrt{1-\frac{\lambda_4^2}{(2\lambda_2+\lambda_3)^2}}\right)\\
&\quad + \sqrt{\left(\lambda_1 - \frac{\lambda_4^2}{2\lambda_2+\lambda_3}\right)(2\rho_1+\rho_2)} > 0\,,\\
&\alpha_1 - 2|\alpha_2|\frac{|\lambda_4|}{2\lambda_2+\lambda_3} + \frac{\alpha_3}{2}\left(1 \pm \sqrt{1-\frac{\lambda_4^2}{(2\lambda_2+\lambda_3)^2}}\right) + \frac{\alpha_4}{2}\left(1 \mp \sqrt{1-\frac{\lambda_4^2}{(2\lambda_2+\lambda_3)^2}}\right)\\
&\quad + \sqrt{\left(\lambda_1 - \frac{\lambda_4^2}{2\lambda_2+\lambda_3}\right)\rho_1} > 0\,.
\end{aligned} \tag{B.12}$$

JHEP03(2023)168

- For $\beta = 1$, $\sin\omega = 0$,

$$\alpha_1 - 2|\alpha_2| + \frac{\alpha_3}{2} + \frac{\alpha_4}{2} + \sqrt{(\lambda_1 + \lambda_3 + 2(\lambda_2 - |\lambda_4|))(2\rho_1 + \rho_2)} > 0\,,$$
$$\alpha_1 - 2|\alpha_2| + \frac{\alpha_3}{2} + \frac{\alpha_4}{2} + 2\sqrt{(\lambda_1 + \lambda_3 + 2(\lambda_2 - |\lambda_4|))\rho_1} > 0\,. \tag{B.13}$$

- For $\beta = 1$, $\cos\omega = -\lambda_4/2\lambda_2$,

$$\alpha_1 - 2|\alpha_2| + \frac{\alpha_3}{2} + \frac{\alpha_4}{2} + \sqrt{\left(\lambda_1 + \lambda_3 - 2\lambda_2 - \frac{\lambda_4^2}{4\lambda_2}\right)(2\rho_1 + \rho_2)} > 0\,,$$
$$\alpha_1 - 2|\alpha_2| + \frac{\alpha_3}{2} + \frac{\alpha_4}{2} + 2\sqrt{\left(\lambda_1 + \lambda_3 - 2\lambda_2 - \frac{\lambda_4^2}{4\lambda_2}\right)\rho_1} > 0\,. \tag{B.14}$$

Eqs. (B.6), (B.7), (B.11), (B.12), (B.13), and (B.14) together constitute the full set boundedness from below conditions in DLRSM.

References

[1] J.C. Pati and A. Salam, *Lepton Number as the Fourth Color*, *Phys. Rev. D* **10** (1974) 275 [INSPIRE].

[2] R.N. Mohapatra and J.C. Pati, *A Natural Left-Right Symmetry*, *Phys. Rev. D* **11** (1975) 2558 [INSPIRE].

[3] R.N. Mohapatra and J.C. Pati, *Left-Right Gauge Symmetry and an Isoconjugate Model of CP Violation*, *Phys. Rev. D* **11** (1975) 566 [INSPIRE].

[4] G. Senjanovic and R.N. Mohapatra, *Exact Left-Right Symmetry and Spontaneous Violation of Parity*, *Phys. Rev. D* **12** (1975) 1502 [INSPIRE].

[5] G. Senjanovic, *Spontaneous Breakdown of Parity in a Class of Gauge Theories*, *Nucl. Phys. B* **153** (1979) 334 [INSPIRE].

[6] K.S. Babu and V.S. Mathur, *Radiatively Induced Seesaw Mechanism for Neutrino Masses*, *Phys. Rev. D* **38** (1988) 3550 [INSPIRE].

[7] A. Zee, *A Theory of Lepton Number Violation, Neutrino Majorana Mass, and Oscillation*, *Phys. Lett. B* **93** (1980) 389 [*Erratum ibid.* **95** (1980) 461] [INSPIRE].

[8] K.S. Babu and A. Thapa, *Left-Right Symmetric Model without Higgs Triplets*, arXiv:2012.13420 [INSPIRE].

[9] P. Fileviez Perez and C. Murgui, *Lepton Flavour Violation in Left-Right Theory*, *Phys. Rev. D* **95** (2017) 075010 [arXiv:1701.06801] [INSPIRE].

[10] P. Fileviez Perez, C. Murgui and S. Ohmer, *Simple Left-Right Theory: Lepton Number Violation at the LHC*, *Phys. Rev. D* **94** (2016) 051701 [arXiv:1607.00246] [INSPIRE].

JHEP03(2023)168

[11] V. Bernard, S. Descotes-Genon and L. Vale Silva, *Constraining the gauge and scalar sectors of the doublet left-right symmetric model*, *JHEP* **09** (2020) 088 [arXiv:2001.00886] [INSPIRE].

[12] V. Brdar and A.Y. Smirnov, *Low Scale Left-Right Symmetry and Naturally Small Neutrino Mass*, *JHEP* **02** (2019) 045 [arXiv:1809.09115] [INSPIRE].

[13] P.S.B. Dev, R.N. Mohapatra and Y. Zhang, *Probing the Higgs Sector of the Minimal Left-Right Symmetric Model at Future Hadron Colliders*, *JHEP* **05** (2016) 174 [arXiv:1602.05947] [INSPIRE].

[14] ATLAS collaboration, *Search for a heavy charged boson in events with a charged lepton and missing transverse momentum from pp collisions at* $\sqrt{s} = 13$ *TeV with the ATLAS detector*, *Phys. Rev. D* **100** (2019) 052013 [arXiv:1906.05609] [INSPIRE].

[15] ATLAS collaboration, *Search for high-mass dilepton resonances using* $139\,fb^{-1}$ *of pp collision data collected at* $\sqrt{s} = 13$ *TeV with the ATLAS detector*, *Phys. Lett. B* **796** (2019) 68 [arXiv:1903.06248] [INSPIRE].

[16] CMS collaboration, *Search for resonant and nonresonant new phenomena in high-mass dilepton final states at* $\sqrt{s} = 13$ *TeV*, *JHEP* **07** (2021) 208 [arXiv:2103.02708] [INSPIRE].

[17] H. Georgi and S. Weinberg, *Neutral Currents in Expanded Gauge Theories*, *Phys. Rev. D* **17** (1978) 275 [INSPIRE].

[18] N.G. Deshpande, J.F. Gunion, B. Kayser and F.I. Olness, *Left-right symmetric electroweak models with triplet Higgs*, *Phys. Rev. D* **44** (1991) 837 [INSPIRE].

[19] Particle Data Group collaboration, *Review of Particle Physics*, *PTEP* **2020** (2020) 083C01 [INSPIRE].

[20] J. Chakrabortty, J. Gluza, T. Jelinski and T. Srivastava, *Theoretical constraints on masses of heavy particles in Left-Right Symmetric Models*, *Phys. Lett. B* **759** (2016) 361 [arXiv:1604.06987] [INSPIRE].

[21] J. Chakrabortty, P. Konar and T. Mondal, *Constraining a class of* $B-L$ *extended models from vacuum stability and perturbativity*, *Phys. Rev. D* **89** (2014) 056014 [arXiv:1308.1291] [INSPIRE].

[22] G. Chauhan, *Vacuum Stability and Symmetry Breaking in Left-Right Symmetric Model*, *JHEP* **12** (2019) 137 [arXiv:1907.07153] [INSPIRE].

[23] M. Frank et al., *Vacuum structure of Alternative Left-Right Model*, *JHEP* **03** (2022) 065 [arXiv:2111.08582] [INSPIRE].

[24] K. Kannike, *Vacuum stability conditions and potential minima for a matrix representation in lightcone orbit space*, *Eur. Phys. J. C* **81** (2021) 940 [*Addendum ibid.* **82** (2022) 247] [arXiv:2109.01671] [INSPIRE].

[25] CMS collaboration, *A measurement of the Higgs boson mass in the diphoton decay channel*, *Phys. Lett. B* **805** (2020) 135425 [arXiv:2002.06398] [INSPIRE].

[26] ATLAS collaboration, *A combination of measurements of Higgs boson production and decay using up to* $139\,fb^{-1}$ *of proton-proton collision data at* $\sqrt{s} = 13$ *TeV collected with the ATLAS experiment*, ATLAS-CONF-2020-027 (2020) [INSPIRE].

[27] CMS collaboration, *Combined Higgs boson production and decay measurements with up to* $137\,fb^{-1}$ *of proton-proton collision data at* $\sqrt{s} = 13$ *TeV*, CMS-PAS-HIG-19-005 (2020) [INSPIRE].

JHEP03(2023)168

[28] ATLAS collaboration, *Constraints on the Higgs boson self-coupling from the combination of single-Higgs and double-Higgs production analyses performed with the ATLAS experiment*, ATLAS-CONF-2019-049 (2019) [INSPIRE].

[29] Y. Zhang, H. An, X. Ji and R.N. Mohapatra, *General CP Violation in Minimal Left-Right Symmetric Model and Constraints on the Right-Handed Scale*, *Nucl. Phys. B* **802** (2008) 247 [arXiv:0712.4218] [INSPIRE].

[30] J.F. Gunion and H.E. Haber, *The CP conserving two Higgs doublet model: The Approach to the decoupling limit*, *Phys. Rev. D* **67** (2003) 075019 [hep-ph/0207010] [INSPIRE].

[31] C. Bonilla, R.M. Fonseca and J.W.F. Valle, *Consistency of the triplet seesaw model revisited*, *Phys. Rev. D* **92** (2015) 075028 [arXiv:1508.02323] [INSPIRE].

JHEP03(2023)168